Polypeptide-Functionalized NaYF$_4$:Yb^{3+},Er^{3+} Nanoparticles: Red-Emission Biomarkers for High Quality Bioimaging Using a 915 nm Laser

Ao Xia,[†,‡,§] Yunyun Deng,[‡,§] Huan Shi,[‡] Jin Hu,[‡] Jun Zhang,[‡] Shishan Wu,[†] Qiang Chen,[†] Xiaohua Huang,*[‡] and Jian Shen*[†,‡]

[†]School of Chemistry & Chemical Engineering, Nanjing University, 22 Hankou Road, Nanjing 210093, China

[‡]Jiangsu Collaborative Innovation Center of Biomedical Functional Materials, Jiangsu Key Laboratory of Biomedical Materials, College of Chemistry and Materials Science, Nanjing Normal University, 1 Wenyuan Road, Nanjing 210046, China

Ⓢ *Supporting Information*

ABSTRACT: We prepared poly-L-aspartic acid (PASP) functionalized NaYF$_4$:Yb^{3+},Er^{3+} upconversion nanoparticles (UCNP-PASP). These nanoparticles can give red upconversion emission under excitation at 915 nm, whose wavelength of emission and excitation is located in the optical window of biological tissue. Dynamic laser scatting and zeta potentials of UCNP-PASP were used to study their stabilities in different aqueous solution. To understand the mechanism of the red emission of UCNP-PASP, photoluminescence spectra of samples were recorded before and after modification with PASP, poly acrylic acid (PAA), and poly(ether imide) (PEI) ligands under excitation at 915 and 980 nm, respectively. The cytotoxicity of the UCNP-PASP was also examined on a A549 cell and KB cell by 3-[4,5-dimethylthiazol-2-yl]-2,5-diphenyl-tetrazolium bromide (MTT) assay. Moreover, the PASP-functionalized UCNP was employed as a potential biomarker for in vitro and in vivo experiments of upconversion luminescence imaging.

KEYWORDS: upconversion luminescence, polypeptide, NaYF$_4$, poly-L-aspartic acid, bioimaging
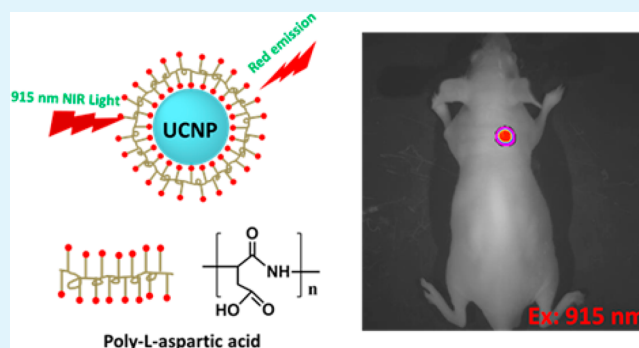
1. INTRODUCTION

Due to the special anti-Stokes emission, upconversion luminescent nanoparticles (UCNP) have been paid great attention in the field of biology and biomedicine, such as molecular detection,[1,2] therapeutics,[3−7] and biological imaging.[8−12] To minimize the overheating effect from the excitation irradiation at 980 nm, interest in the synthesis of aqueous UCNP as biological biomarkers, whose wavelength of emission and excitation is located in the optical window of biological tissue, has been steadily increasing.[13,14] Especially, an aqueous UCNP with red emission is desirable to obtain the deeper penetration and the higher ratio of signal-to-noise (SNR).[15] However, because of the multiple metastable excited states of lanthanide ions, it is difficult to synthesize UCNP with high chromatic purity of red emission.[16]

Recently, several research groups have reported to synthesize UCNP with high purity of upconversion red emission or high ratio of red to green luminescence (RRG). For example, by changing the concentration of the dopant Yb^{3+} or Gd^{3+}, a series of NaYF$_4$:Yb^{3+},Er^{3+} or NaYF$_4$:Gd^{3+},Yb^{3+},Er^{3+} UCNP with different RRG was obtained.[17−19] NaF or Au nanoparticles could enhance the upconversion emission and regulate the RRG of the NaYF$_4$:Yb^{3+},Er^{3+} UCNP.[20,21] When Mn^{2+} as the

dopant ion was introduced to the matrix materials, such as KMnF$_3$ and MnF$_2$, Mn^{2+}-doped UCNP with monochromatic upconversion red emission were synthesized.[22,23] By adjusting the ratio of octadecylamine to oleamide coating nanoparticle surface, the output emission of NaYF$_4$ UCNP was controlled by a given composition of host and single activator under excitation of 980 nm.[24] Although great efforts have been made, it is still a challenge to prepare hydrophilic UCNP with red emission or high RRG for the application of biology and biomedicine, when the biotoxicity and the synthesis protocol of UCNP are considered.[25] To the best of our knowledge, there have been few reports on the polypeptide-functionalized UCNP with red emission for the bioimaging using 915 nm NIR laser as the excitation source up until now, and the wavelength of emission and excitation is located in the optical window of biological tissue ranging from 600 to 950 nm.

Here, we prepared hydrophilic NaYF$_4$:Yb^{3+},Er^{3+} upconversion nanoparticles functionalized with poly-L-aspartic acid (PASP) ligand (UCNP-PASP). Its aqueous stability was

characterized by DLS and zeta potential in simulate physically relevant conditions. And as a biomarker functionalized with poly(amino acid), its cytotoxicity was carefully examined.[26] Notably, when using a 915 nm laser as the excitation source, red emission of UCNP-PASP were obtained at 670 nm. It was an important feature that all wavelengths of the emission and excitation were in the optical window of biological tissue ranging from 600 to 950 nm. Finally, we proved that the red emission UCNP-PASP could be applied as a biomarker for the high quality upconversion luminescence (UCL) bioimaging.

2. EXPERIMENTAL SECTION

2.1. Materials. NH_4F, NaOH, sodium oleate, ethanol, cyclohexane, PAA, PEI, and hydrochloric solution were purchased from Sinopharm Chemical Reagent Co., China. Oleic acid (OA) and octadecene (ODE) were purchased from Alfa Aesar Ltd. Ln_2O_3 (>99.9%, Ln = Y, Yb, and Er) was purchased from Aladin Reagent Co., China. PASP (D_{20}) was ordered and purchased from Ai Keda Biochemical Technology Co., Ltd. 3-[4,5-Dimethylthiazol-2-yl]-2,5-diphenyl-tetra-zolium bromide (MTT) and other biological reagents were purchased from Wangqin Co. All other chemical reagents were of analytical grade and were directly used without further purification. Deionized water was used throughout experiments.

$LnCl_3$ (Ln = Y, Yb, and Er) were prepared by dissolving the corresponding metal oxide in 10% hydrochloric solution and then evaporating the water completely.

2.2. Preparation of OA-Capped $NaYF_4$:Yb^{3+},Er^{3+} Nanocryst-als. Monodispersed OA-capped upconversion luminescence NaY-F_4:Yb^{3+},Er^{3+} nanocrystals (UCNP-OA) were synthesized through a facile coprecipitation protocol as reported.[27,28] In a typical synthesis of UCNP-OA, a mixture of 0.78 mmol of YCl_3, 0.2 mmol of $YbCl_3$, 0.02 mmol of $ErCl_3$, 12 mL of oleic acid, and 15 mL of ODE was added into a 100 mL flask. The resulting mixture was heated to 160 °C until the solution was clear with an inert argon flow. After the solution was cooled down to the room temperature, 10 mL of methanol solution containing 2.5 mmol of NaOH and 4 mmol of NH_4F was added dropwise into the flask. After stirring for 30 min, the solution was slowly heated to 120 °C and degassed for 10 min to remove methanol. Under the argon atmosphere, the solution was heated to 300 °C and maintained for 1 h and then cooled down to room temperature naturally. Finally, UCNP-OA precipitated from the solution with ethanol and then washed with ethanol/water (1:1, v/v) three times.

2.3. Preparation of PASP-Functionalized $NaYF_4$:Yb^{3+},Er^{3+} Nanocrystals. The PASP-functionalized $NaYF_4$:Yb^{3+},Er^{3+} nanocryst-als (UCNP-PASP) were prepared by using a modified ligand exchange strategy. In a typical ligand exchange procedure, 30 mg of PASP was first dissolved in 10 mL of water and vigorously stirred for 30 min at 50 °C. A 10 mg of UCNP-OA was dispersed in a mixed solution of cyclohexane (10 mL) and ethanol (5 mL), and then, the mixture was dropwise added into the PASP solution. When the temperature was maintained at 50 °C, a clear solution was obtained and stirred for 4 h. After cooling to R.T., the lower liquid was collected until the mixture was layered. UCNP-PASP was obtained by centrifugation at 15 000 rpm for 5 min. Finally, the product was washed with ethanol twice and redispersed in 10 mL of water.

2.4. Preparation of UCNP-PAA and UCNP-PEI Nanocrystals. The preparation of UCNP-PAA and UCNP-PEI nanocrystals was similar to that of UCNP-PASP, where the ligand was PAA and PEI, respectively. In a typical procedure, 20 mg of PAA or 35 mg PEI was first dissolved in 10 mL of water and vigorously stirred for 30 min at 50 °C. Ten mg of UCNP-OA was dispersed in a mixed solution of cyclohexane (10 mL) and ethanol (5 mL), and then, the mixture was dropwise added into the PAA or PEI solution and stirred for 4 h. After cooling down to R.T., the lower liquid was collected until the mixture was layered. UCNP-PAA or UCNP-PEI was obtained by centrifuga-tion at 15 000 rpm for 5 min. Finally, the product was washed with ethanol twice and redispersed in 10 mL of water.

2.5. Characterization. Powder X-ray diffraction (XRD) measure-ment of UCNP-OA was carried out on a Bruker D4 X-ray

diffractometer (Cu Kα radiation, λ = 0.15406 nm). Transmission electron microscopy (TEM) and high resolution transmission electron microscopy (HRTEM) experiments were conducted on a JEOL 2010F microscope (Japan) operated at 200 kV. Samples of UCNP-OA and UCNP-PASP for TEM and HRTEM were prepared for morphologies observation by placing a drop of the dilute dispersion on the surface of a copper grid. Thermogravimetric analysis (TGA) of UCNP-OA and UCNP-PASP were carried out with a Pyris 1 thermogravimetric analyzer under air flow with a heating rate of 10 °C/min in range from 100 to 600 °C.[29] Dynamic light scattering (DLS) experiments of UCNP-OA and UCNP-PASP were determined by a Malvern Zetasizer Nano, and also Zeta potential of UCNP-PASP were measured in the saline solution (0.9% NaCl, pH = 7.6). FT-IR spectra of UCNP-OA and UCNP-PASP were collected with Shimadzu IR Prestige-21 spectrometer in KBr pellets. Upconversion luminescence (UCL) spectra were collected on an Edinburgh LFS-920 spectrometer with external 0−1 W adjustable CW lasers at 915 and 980 nm, respectively, where all the concentrations of UCNP-OA and UCNP-PASP was 500 μg/mL. UCL images were digitally acquired on a small animal imaging system equipped with CW lasers at 915 and 980 nm, respectively.

2.6. In Vitro UCL Imaging. Polypeptide-functionalized UCNP-PASP solution (10 mg/mL) was diluted with 1% warm agarose solutions at the concentrations of 0.125, 0.25, 0.5, and 1 mg/mL, and then transferred into a 96-well plate (100 μL for each well). After cooling to room temperature, the agarose solutions containing the nanoparticles gelated in the well of plates. For the upconversion luminescent imaging, the microplate was covered with a 1 mm thick of beef tissue. Upconversion luminescence images of UCNP-PASP gel plates covered with beef tissue were acquired with an in vivo imaging system using a 980 nm laser and a 915 nm laser as the excitation sources, and intensities of UCL signals were analyzed with the Kodak Molecular Imaging Software. The laser power density was 150 mW/cm² during imaging.

2.7. Cell Culture. A549 cell lines and KB cell lines were purchased by the Institute of Basic Medical Sciences, Chinese Academy of Medical Sciences. Cells were grown in modified Eagle's medium (MEM) supplemented with 10% fetal bovine serum (FBS) and 1% insulin (10 mL, 400 units) at 37 °C under a humidified atmosphere containing 5% CO_2.

2.8. Cytotoxicity Assay of UCNP-PASP. Cytotoxicity of UCNP-PASP was determined by the MTT assay with A549 cells and KB cells. Cells were seeded into a 96-well cell culture plate at 5×10^4/well and incubated at 37 °C under a humidified atmosphere containing 5% CO_2. The cultured medium was modified with 15% FBS, 100 units/mL penicillin, and 100 unit streptomycin. After incubation for 24 h, the cultured medium with UCNP-PASP nanorods (100 μL/well) at different concentrations of 0, 10, 25, 50, 100, 200, 400, and 800 μg/mL were added to the wells of the treatment group, and RPMI 1640 (100 μL/well) to the negative control group, respectively. The cells were subsequently incubated for 24 h and for 48 h under a humidified atmosphere containing 5% CO_2 at 37 °C, respectively. Thereafter, 10 μL of MTT (5 mg/mL) solution was added to each well and the plate was incubated for an additional 4 h. After the addition of dimethyl sulfoxide (DMSO, 100 μL/well), the assay plate was allowed to stand at room temperature for 20 min. The optical density OD 570 value (Abs.) of each well was measured by means with background subtraction at 690 nm on a Tecan Infinite M200 monochromator-based multifunction microplate reader. The following formula was used to calculate the viability of cell growth:

$$\text{cell viability} = (\text{mean of abs. value of value of treatment group} / \text{mean abs value of control}) \times 100\%$$

2.9. Animals. Animal procedures were in agreement with the guidelines of the regional ethic committee for animal experiments. Nude mouse (female, 6 weeks old, 16−20 g/animal) was purchased from Shanghai SMMU. All animals were housed in standard environment and acclimated for at least 24 h before experiment.

2.10. In Vivo UCL Imaging. UCL imaging in vivo was conducted with UCL imaging system, which was equipped with an external 0−1
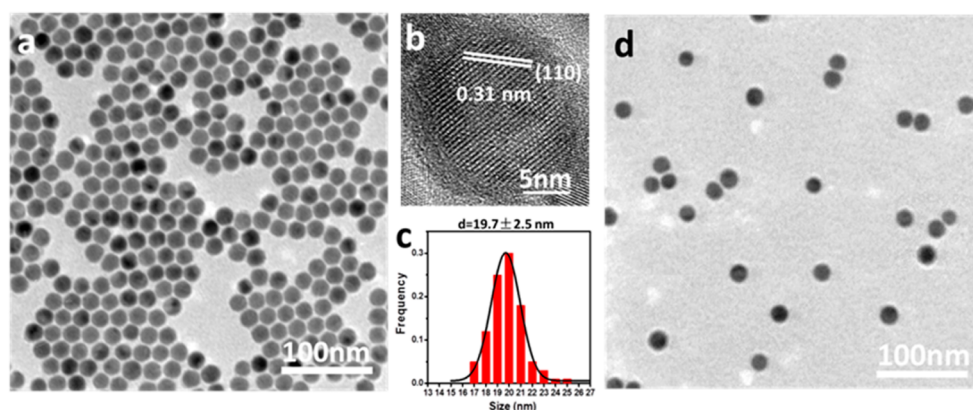
Figure 1. (a) TEM image of UCNP-OA. (b) High resolution TEM image of UCNP-OA. (c) Histograms of the diameter of UCNP-OA. (d) TEM image of UCNP-PASP.
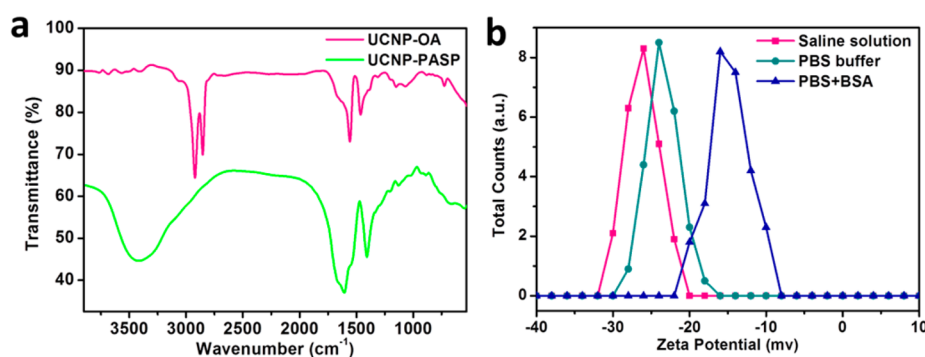

Figure 2. (a) FT-IR spectra of UCNP-OA and UCNP-PASP. (b) Zeta potentials of UCNP-PASP dispersed in 0.9% NaCl saline solution, PBS buffer, and PBS + BSA solution.

W adjustable CW infrared laser and an Andor DU897 EMCCD. UCL images were obtained with a low-pass filter at 850 nm, and intensities of UCL signals were analyzed with the Kodak Molecular Imaging Software.

Nude mice were anesthetized with 100 μL of 10% chloral hydrate. After 100 μL of PBS containing 2 mg of UCNP-PASP were subcutaneously injected under upper right skin of the nude mouse, a whole-body UCL imaging was performed with external 150 mW/cm^2 CW infrared laser at 915 and 980 nm, respectively.

3. RESULTS AND DISCUSSION

3.1. Preparation and Characterization of UCNP-PASP Nanocrystals. Monodispersed UCNP-OA nanocrystal is usually prepared at 300 °C via a modified coprecipitation strategy. Due to its surface capped with the OA as ligands, the as-prepared nanocrystal is hydrophobic and can be steadily dispersed in the nonpolar organic solvent, such as cyclohexane and chloroform. Transmission electron microscope (TEM) image (Figure 1a) clearly shows that those nanocrystals are uniform and well arrayed on the copper grid. High resolution TEM (HR-TEM) (Figure 1b) reveals the nanocrystal is composed of lattice fringes indexed as (110) planes with an interplanar spacing of 0.31 nm, confirming that the as-prepared particles have a good crystallization as previously report.[30] By measuring the diameter of 100 nanocrystals imaged by TEM, UCNP-OA has a mean diameter of 19.8 ± 2.5 nm (Figure 1c).

To obtain a hydrophilic nanoparticle for the application of in vitro or in vivo UCL imaging, a ligand exchange procedure is employed to functionalize UCNP with the polypeptide. A carboxyl polypeptide, PASP, replaces OA ligand on the surface of UCNP in a mixture solvent of water, ethanol, and

cyclohexane at 50 °C. X-ray diffraction (XRD) analysis is carried out to determine the crystallinity of the UCNP-PASP. The diffraction peaks of UCNP-PASP (Figure S1, Supporting Information) are obviously broad due to their small size on the nanoscale. These positions of main diffraction peaks of UCNP-PASP sample agree with the standard hexagonal-phase NaYF$_4$ crystal (JCPDS 16-0334) very well, and no diffraction peak of NaF crystal and cubic phase of NaYF$_4$ crystal is found.[31,32] Furthermore, a TEM image (Figure 1d) shows that UCNP-PASP is dispersed well in water without aggregations after ligands exchanging.

FT-IR spectra (Figure 2a) of UCNP-OA and UCNP-PASP present the IR absorption of samples before and after surface modification of the UCNP. For the UCNP-OA, the multipeak bands at 2925 and 2855 cm^{-1} can be assigned to the stretching vibrations of CH$_2$. After the surface modification with PASP, two strong peaks at 1608 and 1422 cm^{-1}, found in the FT-IR spectrum of UCNP-PASP, correspond to the −CONH− bending vibration and COO$^-$ symmetrical stretching vibration, respectively. These findings suggest that PASP has been successfully coated onto the surface of the UCNP. Furthermore, the surface PASP layer was investigated by thermogravimetric analysis (TGA). TGA curves of the UCNP capped with OA and UCNP-PASP are illustrated in Figure S2, and the weight loss of OA and PASP on the surface of UCNP was 13.6% and 23.8%, respectively. These results further infer that PASP has successfully replaced OA on the surface of UCNP by the ligand exchange process, and this finding agrees with the FT-IR results.
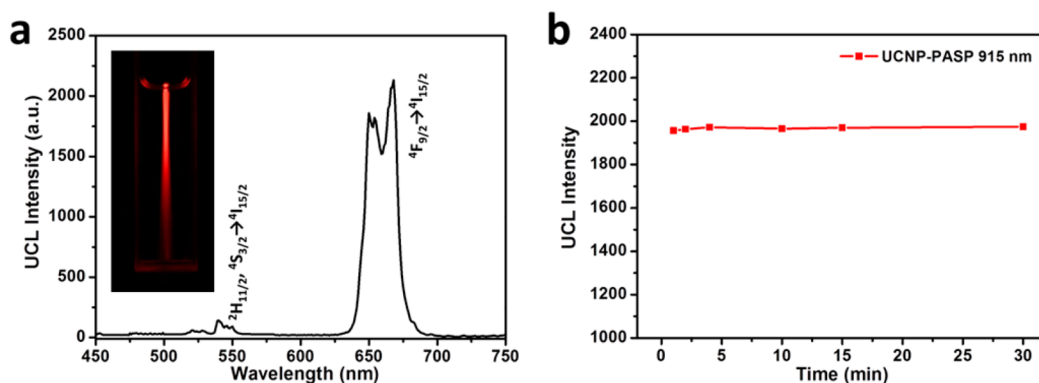
Figure 3. (a) UCL spectrum and digital picture of UCNP-PASP dispersed in the saline solution under the excitation at 915 nm. (b) Photostability of UCNP-PASP dispersed in the saline solution under the excitation at 915 nm. The power density of CW laser at 915 nm is 400 mW/cm^2.
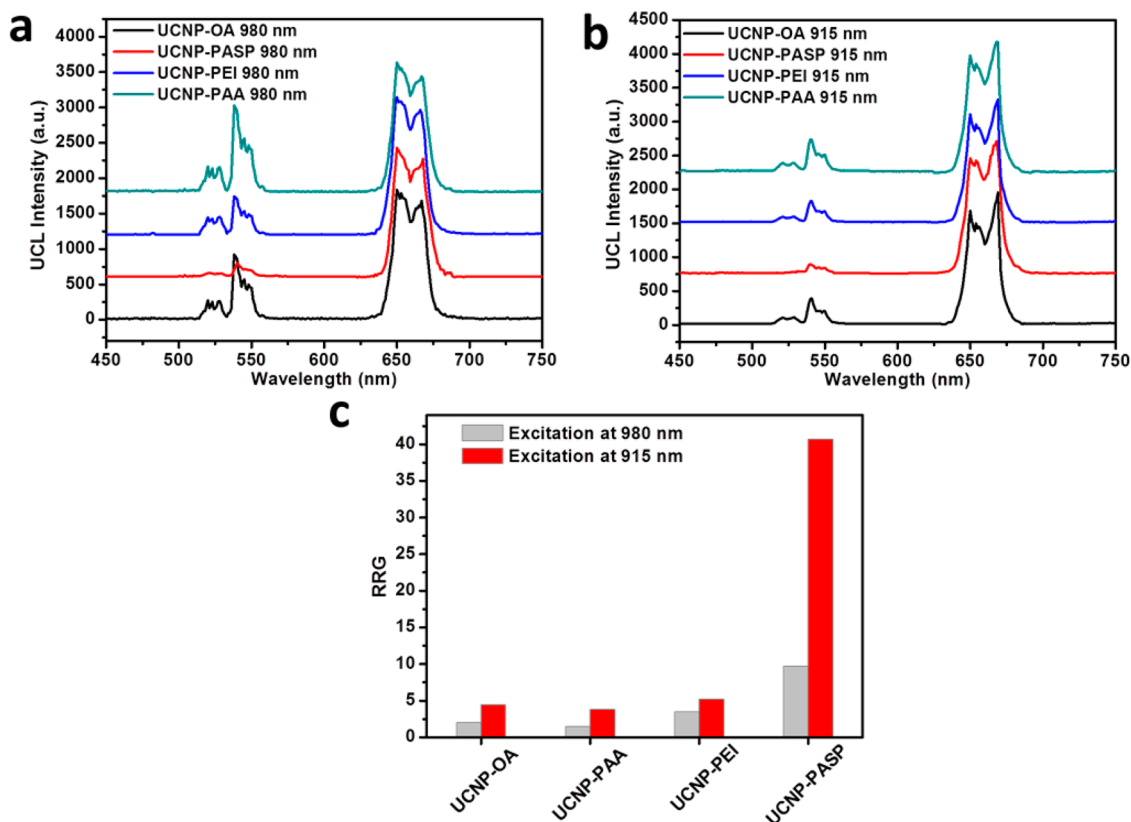

Figure 4. (a) UCL spectra of UCNP-OA, UCNP-PASP, UCNP-PEI, and UCNP-PAA under the excitation at 980 nm. (b) UCL spectra of UCNP-OA, UCNP-PASP, UCNP-PEI, and UCNP-PAA under the excitation at 915 nm. (c) RRG of UCNP-OA, UCNP-PAA, UCNP-PEI, and UCNP-PASP under the excitation at 980 and 915 nm, respectively. All the power density for CW laser is 400 mW/cm^2 at 980 and 915 nm.

To investigate the stability of UCNP-PASP in aqueous solution, dynamic light scattering (DLS) was used to characterize the size of UCNP-PASP in simulate physically relevant conditions (Figure S3). The hydrodynamic diameter of UCNP-PASP was 25.4 ± 3.2 and 30.1 ± 6.1 nm in the saline and the 4% BSA PBS solutions, respectively. The DLS diameter of UCNP-PASP is largest in the 4% BSA PBS solution, but no aggregation of nanoparticles is found. It is probably resulted from interaction between the PASP ligand and BSA proteins.[33] Furthermore, zeta potentials of UCNP-PASP was measured to understand the effect of ion strength and protein absorption in the saline, PBS and 4% BSA PBS solution. As show in Figure 2b, the zeta potentials of UCNP-PASP are about −27.2, −24.5, and −14.6 mV in saline, PBS and 4% BSA PBS solution,

respectively. Its zeta potential slightly decreases with the increase in pH of the corresponding solvent. When dispersed with 4% BSA in PBS solution, the zeta potential of UCNP-PASP is lowest and supposed to interaction with BSA proteins, and it agrees with the result of DLS. Therefore, based on results of the DLS and the zeta potentials, no aggregation of nanoparticles, resulting from pH, ionic strength, and protein absorption, was observed or expected when UCNP was functionalized with the PASP as ligand.

3.2. UCL Properties of UCNP-PASP Nanocrystals. The upconversion luminescence properties of UCNP-PASP were also studied under the excitation at 915 nm. As shown in the digital photograph (Figure 3a, inset), strong red light illuminates the whole quartz cuvette when UCNP-PASP is
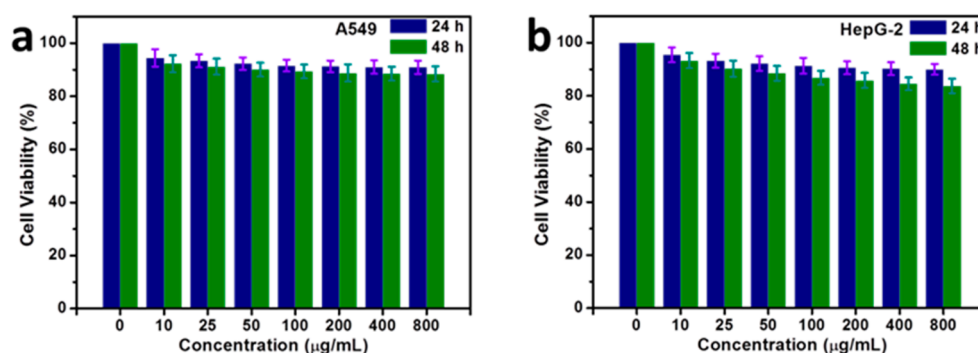
Figure 5. Cytotoxicity test of as-prepared UCNP-PASP on the viability of (a) A549 and (b) KB cells incubated with different concentrations of UCNP-PASP, as measured by MTT assay.
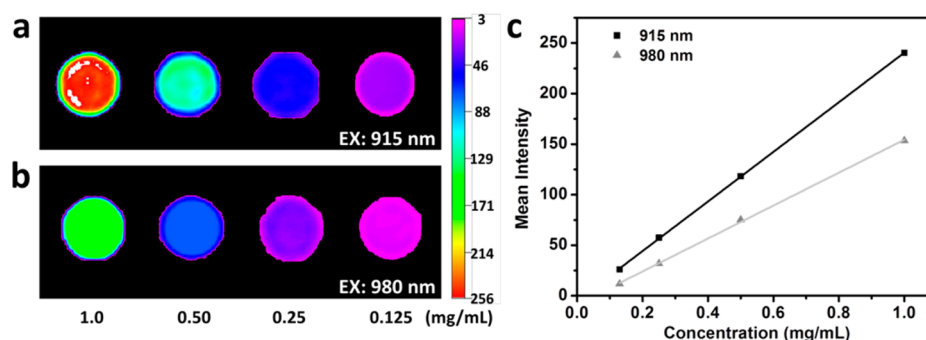

Figure 6. In vitro upconversion luminescence images of UCNP-PASP gels at the concentrations at 0.125, 0.25, 0.5, and 1.0 mg/mL, when under excitations at (a) 915 and (b) 980 nm. (c) Mean intensities of UCNP-PASP gels under the excitation at 980 and 915 nm, respectively.

excited at 915 nm. On its UCL spectrum (Figure 3a), there is mainly a strong peak centered at 670 nm and a weak peak centered at 545 nm in the visible region. The UC RRGs of UCNP-PASP is about 40.7 under the excitation at 915 nm. Two emission peaks could be assigned to $^{2}H_{11/2}$, $^{4}S_{3/2} \rightarrow {}^{4}I_{15/2}$, and $^{4}F_{9/2} \rightarrow {}^{4}I_{15/2}$ of Er^{3+} transitions, respectively, where the dopant Yb^{3+} acted as an NIR absorber and efficiently transferred energy to the emitter Er^{3+}.[31] The photostability of UCNP-PASP was also examined with time when excited by a 915 nm. As shown in Figure 3b, there is no obvious intensity decline of UC emission of UCNP-PASP for 30 min. UCNP-PASP exhibits neither photoblinking on the minute time scales nor photobleaching even with half an hour of continuous excitation.[34]

To further understand the mechanism of the red emission of UCNP-PASP, we synthesize UCNP-PAA and UCNP-PEI as comparison. And their upconversion luminescence spectra were measured before and after the surface modification under the continuous wave (CW) NIR excitation at 915 and 980 nm, respectively. As shown in Figure 4a and b, there are mainly two UCL peaks on the UCL spectra for all samples under the excitation at 980 and 915 nm, which were centered at 545 and 670 nm, respectively.[35] However, under the different excitation wavelength, the RRGs are different for UCNP-OA, UCNP-PASP, UCNP-PAA, and UCNP-PEI samples, which are ranged from 1.5 to 40 (Figure 4c). Comparison with the spectra of UCNP-OA at the same excitation wavelength, the RRGs of samples varied with the ligand on the surface of UCNP nanocrystals.[36] For the UCNP-PASP, its RRG is about 40 and highest in all of samples when excited by a 915 nm laser, and its upconversion emission is nearly red color. In addition to the UCNP-PAA, its RRG is less than that of the original OA ligand,

and the PAA ligand is more benefit to green emission than red emission relative to the OA ligand.[37] It is an interesting finding that RRG of UC emission can be regulated by the ligand on the surface of UCNP nanocrystals and the excitation wavelength together. Because the green emission or the red emission of UCNPs is two photons process, the excitation wavelength can not only change the population of $^{4}S_{3/2}$ and $^{4}F_{9/2}$ of Er^{3+}, but also affect the nonradiative relaxation from $^{4}S_{3/2}$ to $^{4}F_{9/2}$ of Er^{3+}, which is relative to the size-related phonon-mediated processes in emitting ions.[38] As to the various RRGs of sample with different ligand, it mainly results from the nonradiative relaxation from $^{4}S_{3/2}$ to $^{4}F_{9/2}$ of Er^{3+}.[39]

3.3. Cytotoxicity of UCNP-PASP. One important application of UCNP-PASP is used to be suitable luminescent biomarkers for living labeling and imaging. The cytotoxicity of UCNP-PASP must be carefully estimated. The MTT protocol was employed to evaluate cell viability with UCNP-PASP.[40] The cell viabilities of A549 cells and KB cells were calculated by measuring the activity of NADH-dependent cellular oxidoreductase in cells after 24 and 48 h when incubated with UCNP-PASP. As shown in Figure 5, all the viabilities of A549 cells and KB cells were greater than 80% viable at the 24 h time point when the concentration of UCNP-PASP was less than 800 μg/mL. The number of viable A549 cells was higher than KB cells at both the 24 and 48 h time points when incubated with same concentration of UCNP-PASP. However, even when exposed to the highest concentration of UCNP-PASP, all cells viabilities were greater than 80%. Therefore, UCNP-PASP can be considered to have a relatively low cytotoxicity at concentrations less than 800 μg/mL.

3.4. In Vitro UCL Imaging. When under the excitation at 915 nm, all of the excitation and emission wavelengths of
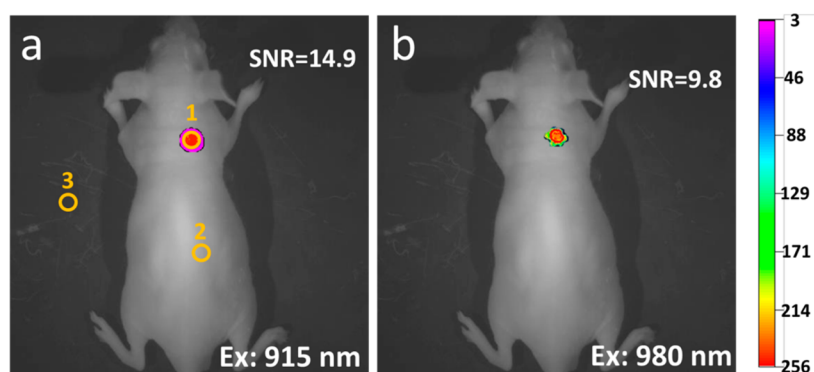
Figure 7. In vivo upconversion luminescence imaging of the living nude mouse with subcutaneous injection of 0.1 mL of UCNPUCNP-PASP under different excitation laser at (a) 915 and (b) 980 nm. Signal-to-noise ratio (SNR) = [(mean luminescence intensity of ROI 1) − (mean luminescence intensity of background region 3)]/[(mean luminescence intensity of ROI 2) − (mean luminescence intensity of background region 3)]. All images were acquired under the same instrumental conditions, and the power density of the laser is 150 mW/cm^2.

UCNP-PASP fall in optical window of the biological tissue. As an in vitro proof-of-concept experiment, we carried out UCL imaging of UCNP-PASP gels at the different concentrations using 980 and 915 nm lasers as excitation sources, where UCNP-PASP gels were covered by 1 mm thick beef.[41,42] When excited at 915 nm (Figure 6a), the UCNP-PASP gels can be visualized even at the concentration of 0.125 mg/mL, and their brightness decreased with a decrease at the concentration of UCNP-PASP. As shown in Figure 6b, when using a 980 nm laser, the brightness of UCNP-PASP gels also clearly changed with the concentration. And the mean intensities of UCNP-PASP gels' UCL were measured and curved in Figure 6c, when under excitations at 915 and 980 nm. The mean intensities of UCL were linear with the concentration of UCNP-PASP. In stark contrast, the mean intensities of UCL under excitations at 915 nm were higher than those under excitations at 980 nm at the same concentration of UCNP-PASP. It can be attributed to low loss of the 915 nm laser and rapid attenuation of the green emission relative to red emission in tissue. Herein, high RRG of UCNP-PASP and excitation at 915 nm will contribute to a higher SNR and deeper penetration in UCL in vitro imaging.

3.5. In Vivo UCL Imaging. High RRG of UC emission and excitation at 915 nm will contribute to a higher SNR and deeper penetration in UCL imaging in vivo because of the optical window of biological tissue. As luminescent biomarkers for biolabeling and bioimaging, the experiment of in vivo UCL imaging was carried out with subcutaneous injection of UCNP-PASP on a nude mouse under the excitation at 915 and 980 nm, respectively.[43] When excited at 915 nm, the in vivo UCL image of the nude mouse was acquired, where a strong UCL signal was easily detected on the top right of the mouse back (Figure S4b). The SNR of the image (Figure 7a) was calculated by measuring the mean intensities of UCL in ROI 1, ROI 2, and ROI 3, respectively.[44] The mean intensities of UCL in ROI 1, ROI 2, and ROI 3 are about 251, 28, and 12, respectively. The SNR of the in vivo NIR-to-NIR UCL imaging is calculated to be about 14.9. Furthermore, no obvious harmful effects on the mice backs were observed from laser exposure at this power density even after 5 min (Figure S4a). As a comparison, the in vivo UCL image under excitation at 980 nm was also acquired on the same nude mouse with same the power density of excitation as that at 915 nm. As shown in Figure S4c, the UCL signal can also be detected in ROI 1 at the same place as that of 915 nm. And the SNR of the in vivo UCL image (Figure 7b) is calculated to be 9.8 under the excitation at 980 nm. Thus, the

UCNP-PASP can be applied as a potential biomarker with higher SNR for in vivo imaging when using the 915 nm laser as the excitation source.

4. CONCLUSION

We have prepared monodispersed UCNP-PASP, which can emit red light when excited by a CW NIR laser at 915 nm. The PASP ligand can stabilize UCNP well in aqueous solution. Cytotoxicity experiments confirm that UCNP-PASP is of very low toxicity for bioapplications. The excitation at 915 nm could achieve higher SNR for in vitro UCL imaging than that of excitation at 980 nm. High quality UCL images of small animal are also obtained, because the UCNP-PASP's emission and excitation is located in the optical window of biological tissue together. Our results provide a strategy to fabricate polypeptide-functionalized UCNP and support the potential application of UCNP-PASP as a promising red emission biomarker for in vitro and in vivo UCL imaging.

■ ASSOCIATED CONTENT

ⓢ Supporting Information

Additional experimental data collected on XRD, TGA, DLS, and in vivo UCL imaging of small animal. This material is available free of charge via the Internet at http://pubs.acs.org.

■ AUTHOR INFORMATION

Corresponding Authors

*E-mail: huangxiaohuabio@hotmail.com (X.H.).
*E-mail: shenjianbio@hotmail. Fax: +86 25 83599188 (S.J.).

Author Contributions

§A.X. and Y.D. contributed equally to this work.

Notes

The authors declare no competing financial interest.

■ REFERENCES

(1) Zhang, F.; Haushalter, R. C.; Haushalter, R. W.; Shi, Y.; Zhang, Y.; Ding, K.; Zhao, D.; Stucky, G. D. Rare-Earth Upconverting Nanobarcodes for Multiplexed Biological Detection. *Small* **2011**, *7*, 1972−1976.

(2) Wu, Y.-M.; Cen, Y.; Huang, L.-J.; Yu, R.-Q.; Chu, X. Upconversion Fluorescence Resonance Energy Transfer Biosensor for Sensitive Detection of Human Immunodeficiency Virus Antibodies in Human Serum. *Chem. Commun.* **2014**, *50*, 4759−4762.

(3) Zhao, L. Z.; Peng, J. J.; Huang, Q.; Li, C. Y.; Chen, M.; Sun, Y.; Lin, Q. N.; Zhu, L. Y.; Li, F. Y. Near- Infrared Photoregulated Drug Release in Living Tumor Tissue via Yolk- Shell Upconversion Nanocages. *Adv. Funct. Mater.* **2014**, *24*, 363−371.

(4) Chen, G. Y.; Qju, H. L.; Prasad, P. N.; Chen, X. Y. Upconversion Nanoparticles: Design, Nanochemistry, and Applications in Theranostics. *Chem. Rev.* **2014**, *114*, 5161−5214.

(5) Cheng, L.; Wang, C.; Ma, X. X.; Wang, Q. L.; Cheng, Y.; Wang, H.; Li, Y. G.; Liu, Z. Multifunctional Upconversion Nanoparticles for Dual-Modal Imaging-Guided Stem Cell Therapy under Remote Magnetic Control. *Adv. Funct. Mater.* **2013**, *23*, 272−280.

(6) Dai, Y. L.; Xiao, H. H.; Liu, J. H.; Yuan, Q. H.; Ma, P. A.; Yang, D. M.; Li, C. X.; Cheng, Z. Y.; Hou, Z. Y.; Yang, P. P.; Lin, J. In Vivo Multimodality Imaging and Cancer Therapy by Near-Infrared Light-Triggered trans-Platinum Pro-Drug-Conjugated Upconverison Nanoparticles. *J. Am. Chem. Soc.* **2013**, *135*, 18920−18929.

(7) Shen, J.; Li, K.; Cheng, L.; Liu, Z.; Lee, S.-T.; Liu, J. Specific Detection and Simultaneously Localized Photothermal Treatment of Cancer Cells Using Layer-by-Layer Assembled Multifunctional Nanoparticles. *ACS Appl. Mater. Interfaces* **2014**, *6*, 6443−6452.

(8) Zeng, S. J.; Wang, H. B.; Lu, W.; Yi, Z. G.; Rao, L.; Liu, H. R.; Hao, J. H. Dual-Modal Upconversion Fluorescent/X-ray Imaging Using Ligand-Free Hexagonal Phase NaLuF₄:Gd/Yb/Er Nanorods for Blood Vessel Visualization. *Biomaterials* **2014**, *35*, 2934−2941.

(9) Ong, L. C.; Ang, L. Y.; Alonso, S.; Zhang, Y. Bacterial Imaging with Photostable Upconversion Fluorescent Nanoparticles. *Biomaterials* **2014**, *35*, 2987−2998.

(10) Yi, Z.; Zeng, S.; Lu, W.; Wang, H.; Rao, L.; Liu, H.; Hao, J. Synergistic Dual-Modality in Vivo Upconversion Luminescence/X-ray Imaging and Tracking of Amine-Functionalized NaYbF₄:Er Nanoprobes. *ACS Appl. Mater. Interfaces* **2014**, *6*, 3839−3846.

(11) Xia, A.; Gao, Y.; Zhou, J.; Li, C. Y.; Yang, T. S.; Wu, D. M.; Wu, L. M.; Li, F. Y. Core-Shell NaYF₄:Yb³⁺,Tm³⁺@FeₓOᵧ Nanocrystals for Dual-Modality T-2-Enhanced Magnetic Resonance and NIR-to-NIR Upconversion Luminescent Imaging of Small-Animal Lymphatic Node. *Biomaterials* **2011**, *32*, 7200−7208.

(12) Liu, S.; Zhang, L.; Yang, T.; Yang, H.; Zhang, K. Y.; Zhao, X.; Lv, W.; Yu, Q.; Zhang, X.; Zhao, Q.; Liu, X.; Huang, W. Development of Upconversion Luminescent Probe for Ratiometric Sensing and Bioimaging of Hydrogen Sulfide. *ACS Appl. Mater. Interfaces* **2014**, *6*, 11013−11017.

(13) Wang, Y. F.; Liu, G. Y.; Sun, L. D.; Xiao, J. W.; Zhou, J. C.; Yan, C. H. Nd³⁺-Sensitized Upconversion Nanophosphors: Efficient In Vivo Bioimaging Probes with Minimized Heating Effect. *ACS Nano* **2013**, *7*, 7200−7206.

(14) Zhan, Q.; Qian, J.; Liang, H.; Somesfalean, G.; Wang, D.; He, S.; Zhang, Z.; Andersson-Engels, S. Using 915 nm Laser Excited Tm³⁺/Er³⁺/Ho³⁺-Doped NaYbF₄ Upconversion Nanoparticles for in Vitro and Deeper in Vivo Bioimaging without Overheating Irradiation. *ACS Nano* **2011**, *5*, 3744−3757.

(15) Tian, G.; Gu, Z. J.; Zhou, L. J.; Yin, W. Y.; Liu, X. X.; Yan, L.; Jin, S.; Ren, W. L.; Xing, G. M.; Li, S. J.; Zhao, Y. L. Mn²⁺ Dopant-Controlled Synthesis of NaYF₄:Yb/Er Upconversion Nanoparticles for in vivo Imaging and Drug Delivery. *Adv. Mater.* **2012**, *24*, 1226−1231.

(16) Wang, F.; Liu, X. G. Multicolor Tuning of Lanthanide-Doped Nanoparticles by Single Wavelength Excitation. *Acc. Chem. Res.* **2014**, *47*, 1378−1385.

(17) Wang, F.; Liu, X. Upconversion Multicolor Fine-Tuning: Visible to Near-Infrared Emission from Lanthanide-Doped NaYF₄ Nanoparticles. *J. Am. Chem. Soc.* **2008**, *130*, 5642−5643.

(18) Zhao, J.; Sun, Y.; Kong, X.; Tian, L.; Wang, Y.; Tu, L.; Zhao, J.; Zhang, H. Controlled Synthesis, Formation Mechanism, and Great Enhancement of Red Upconversion Luminescence of NaYF₄:Yb³⁺, Er³⁺ Nanocrystals/Submicroplates at Low Doping Level. *J. Phys. Chem. B* **2008**, *112*, 15666−15672.

(19) Deng, M.; Wang, L. Unexpected Luminescence Enhancement of Upconverting Nanocrystals by Cation Exchange with Well Retained Small Particle Size. *Nano Res.* **2014**, *7*, 782−793.

(20) Li, H.; Wang, L. Controllable Multicolor Upconversion Luminescence by Tuning the NaF Dosage. *Chem.—Asian J.* **2014**, *9*, 153−157.

(21) Tu, N.; Wang, L. Surface Plasmon Resonance Enhanced Upconversion Luminescence in Aqueous Media for TNT Selective Detection. *Chem. Commun.* **2013**, *49*, 6319−6321.

(22) Wang, J.; Wang, F.; Wang, C.; Liu, Z.; Liu, X. G. Single-Band Upconversion Emission in Lanthanide-Doped KMnF₃ Nanocrystals. *Angew. Chem., Int. Ed.* **2011**, *50*, 10369−10372.

(23) Bai, Z. H.; Lin, H.; Johnson, J.; Gui, S. C. R.; Imakita, K.; Montazami, R.; Fujii, M.; Hashemi, N. The Single-Band Red Upconversion Luminescence from Morphology and Size Controllable Er³⁺/Yb³⁺ Doped MnF₂ Nanostructures. *J. Mater. Chem. C* **2014**, *2*, 1736−1741.

(24) Niu, W. B.; Wu, S. L.; Zhang, S. F. A Facile and General Approach for the Multicolor Tuning of Lanthanide-Ion Doped NaYF₄ Upconversion Nanoparticles within a Fixed Composition. *J. Mater. Chem.* **2010**, *20*, 9113−9117.

(25) Jin, J. F.; Gu, Y. J.; Man, C. W. Y.; Cheng, J. P.; Xu, Z. H.; Zhang, Y.; Wang, H. S.; Lee, V. H. Y.; Cheng, S. H.; Wong, W. T. Polymer-Coated NaYF₄:Yb³⁺, Er³⁺ Upconversion Nanoparticles for Charge-Dependent Cellular Imaging. *ACS Nano* **2011**, *5*, 7838−7847.

(26) Huang, S.; Bai, M.; Wang, L. General and Facile Surface Functionalization of Hydrophobic Nanocrystals with Poly(amino acid) for Cell Luminescence Imaging. *Sci. Rep.* **2013**, *3*, 2023−2028.

(27) Wang, F.; Han, Y.; Lim, C. S.; Lu, Y. H.; Wang, J.; Xu, J.; Chen, H. Y.; Zhang, C.; Hong, M. H.; Liu, X. G. Simultaneous Phase and Size Control of Upconversion Nanocrystals through Lanthanide Doping. *Nature* **2010**, *463*, 1061−1065.

(28) Li, Z.; Zhang, Y.; Jiang, S. Multicolor Core/Shell-Structured Upconversion Fluorescent Nanoparticles. *Adv. Mater.* **2008**, *20*, 4765−4769.

(29) Ma, Y.; Huang, S.; Deng, M.; Wang, L. White Upconversion Luminescence Nanocrystals for the Simultaneous and Selective Detection of 2,4,6-Trinitrotoluene and 2,4,6-Trinitrophenol. *ACS Appl. Mater. Interfaces* **2014**, *6*, 7790−7796.

(30) Zeng, J. H.; Su, J.; Li, Z. H.; Yan, R. X.; Li, Y. D. Synthesis and Upconversion Luminescence of Hexagonal-Phase NaYF₄:Yb³⁺,Er³⁺, Phosphors of Controlled Size and Morphology. *Adv. Mater.* **2005**, *17*, 2119−2123.

(31) Yi, G. S.; Chow, G. M. Synthesis of Hexagonal-Phase NaYF₄:Yb,Er and NaYF₄:Yb,Tm Nanocrystals with Efficient Up-Conversion Fluorescence. *Adv. Funct. Mater.* **2006**, *16*, 2324−2329.

(32) Deng, M.; Ma, Y.; Huang, S.; Hu, G.; Wang, L. Monodisperse Upconversion NaYF₄ Nanocrystals: Syntheses and Bioapplications. *Nano Res.* **2011**, *4*, 685−694.

(33) George, M.; Abraham, T. E. Polyionic Hydrocolloids for the Intestinal Delivery of Protein Drugs: Alginate and Chitosan - A Review. *J. Controlled Release* **2006**, *114*, 1−14.

(34) Nam, S. H.; Bae, Y. M.; Park, Y. I.; Kim, J. H.; Kim, H. M.; Choi, J. S.; Lee, K. T.; Hyeon, T.; Suh, Y. D. Long-Term Real-Time Tracking of Lanthanide Ion Doped Upconverting Nanoparticles in Living Cells. *Angew. Chem., Int. Ed.* **2011**, *50*, 6093−6097.

(35) Quintanilla, M.; Ren, F.; Ma, D.; Vetrone, F. Light Management in Upconverting Nanoparticles: Ultrasmall Core/Shell Architectures to Tune the Emission Color. *ACS Photonics* **2014**, *1*, 662−669.

(36) Tan, M. C.; Al-Baroudi, L.; Riman, R. E. Surfactant Effects on Efficiency Enhancement of Infrared-to-Visible Upconversion Emissions of NaYF₄:Yb-Er. *ACS Appl. Mater. Interfaces* **2011**, *3*, 3910−3915.

(37) Shao, W.; Hua, R.; Zhang, W.; Tian, Y.; Zhao, J.; Na, L.; Yu, J.; Sun, Z. Hydrothermal Synthesis of Poly(acrylic acid)-Functionalized α-(β-)NaYF$_4$:Yb, Er Up-Conversion Nano-/Micro-Phosphors. *Powder Technol.* **2013**, *237*, 326−332.

(38) Schietinger, S.; Menezes, L. d. S.; Lauritzen, B.; Benson, O. Observation of Size Dependence in Multicolor Upconversion in Single Yb^{3+}, Er^{3+} Codoped NaYF$_4$ Nanocrystals. *Nano Lett.* **2009**, *9*, 2477−2481.

(39) Mai, H.-X.; Zhang, Y.-W.; Sun, L.-D.; Yan, C.-H. Highly Efficient Multicolor Up-Conversion Emissions and Their Mechanisms of Monodisperse NaYF$_4$:Yb,Er Core and Core/Shell-Structured Nanocrystals. *J. Phys. Chem. C* **2007**, *111*, 13721−13729.

(40) Jalil, R. A.; Zhang, Y. Biocompatibility of Silica Coated NaYF$_4$ Upconversion Fluorescent Nanocrystals. *Biomaterials* **2008**, *29*, 4122−4128.

(41) Dong, N.-N.; Pedroni, M.; Piccinelli, F.; Conti, G.; Sbarbati, A.; Ramírez-Hernández, J. E.; Maestro, L. M.; Iglesias-de la Cruz, M. C.; Sanz-Rodriguez, F.; Juarranz, A.; Chen, F.; Vetrone, F.; Capobianco, J. A.; Solé, J. G.; Bettinelli, M.; Jaque, D.; Speghini, A. NIR-to-NIR Two-Photon Excited CaF$_2$:Tm^{3+},Yb^{3+} Nanoparticles: Multifunctional Nanoprobes for Highly Penetrating Fluorescence Bio-Imaging. *ACS Nano* **2011**, *5*, 8665−8671.

(42) Yang, T.; Sun, Y.; Liu, Q.; Feng, W.; Yang, P.; Li, F. Cubic Sub-20 nm NaLuF$_4$-Based Upconversion Nanophosphors for High-Contrast Bioimaging in Different Animal Species. *Biomaterials* **2012**, *33*, 3733−3742.

(43) Xiong, L. Q.; Chen, Z. G.; Tian, Q. W.; Cao, T. Y.; Xu, C. J.; Li, F. Y. High Contrast Upconversion Luminescence Targeted Imaging in vivo Using Peptide-Labeled Nanophosphors. *Anal. Chem.* **2009**, *81*, 8687−8694.

(44) Xia, A.; Chen, M.; Gao, Y.; Wu, D. M.; Feng, W.; Li, F. Y. Gd^{3+} Complex-Modified NaLuF$_4$-Based Upconversion Nanophosphors for Trimodality Imaging of NIR-to-NIR Upconversion Luminescence, X-Ray Computed Tomography and Magnetic Resonance. *Biomaterials* **2012**, *33*, 5394−5405.

18336

dx.doi.org/10.1021/am5057272 | *ACS Appl. Mater. Interfaces* 2014, 6, 18329−18336